GLIA

WILEY

RESEARCH ARTICLE

Sublamina-specific organization of the blood brain barrier in the mouse olfactory nerve layer

Antonia Beiersdorfer[1] | Hartwig Wolburg[2] | Janine Grawe[1] | Anja Scheller[3] | Frank Kirchhoff[3] | Christian Lohr[1]

[1]Division of Neurophysiology, University of Hamburg, Hamburg, Germany

[2]Institute of Pathology and Neuropathology, University of Tübingen, Tübingen, Germany

[3]Molecular Physiology, Center for Integrative Physiology and Molecular Medicine (CIPMM), University of Saarland, Homburg, Germany

Correspondence
Antonia Beiersdorfer, Division of Neurophysiology, University of Hamburg, Martin-Luther-King-Pl. 3, Hamburg 20146, Germany.
Email: antonia.beiersdorfer@uni-hamburg.de

Funding information
Christian Lohr, Grant/Award Numbers: LO 779/11, SFB 1328 TP-A07; Frank Kirchhoff, Grant/Award Numbers: FOR 2289 TP-P9, H2020-FET ProAct Neurofibres #732344, SPP 1757/KI 503/12

Abstract

Astrocytes constitute the main glial component of the mammalian blood brain barrier (BBB). However, in the olfactory bulb (OB), the olfactory nerve layer (ONL) is almost devoid of astrocytes, raising the question which glial cells are part of the BBB. We used mice expressing EGFP in astrocytes and tdTomato in olfactory ensheathing cells (OECs), a specialized type of glial cells in the ONL, to unequivocally identify both glial cell types and investigate their contribution to the BBB in the olfactory bulb. OECs were located exclusively in the ONL, while somata of astrocytes were located in deeper layers and extended processes in the inner sublamina of the ONL. These processes surrounded blood vessels and contained aquaporin-4, an astrocytic protein enriched at the BBB. In the outer sublamina of the ONL, in contrast, blood vessels were surrounded by aquaporin-4-negative processes of OECs. Transcardial perfusion of blood vessels with lanthanum and subsequent visualization by electron microscopy showed that blood vessels enwrapped by OECs possessed intact tight junctions. In acute olfactory bulb preparations, injection of fluorescent glucose 6-NBDG into blood vessels resulted in labeling of OECs, indicating glucose transport from the perivascular space into OECs. In addition, Ca^{2+} transients in OECs in the outer sublamina evoked vasoconstriction, whereas Ca^{2+} signaling in OECs of the inner sublamina had no effect on adjacent blood vessels. Our results demonstrate that the BBB in the inner sublamina of the ONL contains astrocytes, while in the outer ONL OECs are part of the BBB.

KEYWORDS

astrocytes, blood brain barrier, neurovascular coupling, olfactory ensheathing cells

1 | INTRODUCTION

The blood brain barrier (BBB) controls as selective barrier transport and diffusion of a plethora of substances from the blood stream into the CNS and vice versa. While transport of nutrients over the BBB is fostered, the entry of noxious substances is blocked. The BBB of capillaries typically consists of endothelial cells (ECs), pericytes, and astrocyte endfeet (Abbott, Patabendige, Dolman, Yusof, & Begley, 2010; Ballabh, Braun, & Nedergaard, 2004). ECs build up the blood vessel wall, are connected with each other by tight junctions to maintain the barrier function and transport glucose from the blood into the perivascular space (Wolburg & Lippoldt, 2002; Zhao, Nelson, Betsholtz, & Zlokovic, 2015). Pericytes support the development of the BBB and stabilize the capillary wall (Bell et al., 2010; Brown et al., 2019; Daneman, Zhou, Kebede, & Barres, 2010). Astrocyte endfeet are mainly involved in metabolic exchange between blood

and neural tissue as well as ion and water regulation. Neuronal information processing consumes about 20% of the total glucose and oxygen demands of the body (Escartin & Rouach, 2013; Harris, Jolivet, & Attwell, 2012). Therefore, efficient metabolic support of neurons is essential. As a cellular component of the BBB, astrocytes take up glucose from the perivascular space, metabolize it and provide lactate to surrounding neurons (Pellerin et al., 2007). In addition, local neuronal activity induces Ca^{2+} signaling in perivascular astrocytes, followed by vasoresponses and changes in local blood flow, a mechanism named neurovascular coupling (Filosa, Bonev, & Nelson, 2004; Gordon, Mulligan, & MacVicar, 2007; Mulligan & MacVicar, 2004; Takano et al., 2006; Zonta et al., 2003). This mechanism is closely associated with a change in glucose supply (neurometabolic coupling; Attwell et al., 2010; Leybaert, 2005). In the olfactory bulb, 2-desoxyglucose autoradiography studies have shown high glucose consumption in the olfactory nerve layer (ONL), an area that harbors thousands of unmyelinated axons of olfactory sensory neurons (OSN), but lacks astrocytic somata (Au, Treloar, & Greer, 2002; Benson, Burd, Greer, Landis, & Shepherd, 1985; Sharp, Kauer, & Shepherd, 1977; Shepherd, 2003). The lack of astrocyte somata and low abundance of astrocytic processes raises the question how the BBB is established in the ONL. A specialized population of glial cell, so-called olfactory ensheathing cells (OECs), is present in the ONL, supporting axonal growth and guidance during development and adult neuroregeneration (Lohr, Grosche, Reichenbach, & Hirnet, 2014). The ONL is divided into an outer and an inner sublamina with physiologically different subpopulations of OECs (Doucette, 1990, 1991; Thyssen et al., 2013). Nonsynaptic release of glutamate and ATP from OSN axons induce Ca^{2+} transients in OECs of the outer ONL, triggering vasoresponses of associated blood vessels, while OECs of the inner ONL lack glutamate- or ATP-evoked Ca^{2+} transients (Rotermund, Schulz, Hirnet, & Lohr, 2019; Thyssen et al., 2010; Thyssen et al., 2013). This indicates intimate structural and functional links between OECs and blood vessels at least in the outer ONL. Hence, this study addresses the question how OECs in the different sublaminae contribute to the BBB. To investigate the cellular components of the BBB in the ONL, we performed electron microscopy studies and immunofluorescence staining using markers for astrocytes (GFAP), astrocyte endfeet (aquaporin 4; AQP4), OECs (S100B) and pericytes (PDGFRβ) in wildtype and transgenic mice expressing tdTomato in OECs (PLP-Cre^ERT2 x tdTomato^fl/fl mice) in OECs and EGFP in astrocytes (hGFAP-EGFP). The results show that blood vessels in the outer ONL are devoid of GFAP- and AQP4-positive structures, but are covered by S100B- and PLP-tdTomato-positive OECs. In contrast, blood vessels in the inner ONL and the glomerular layer (GL) are covered by GFAP- and AQP4-positive cell processes of astrocytes. Pericytes are present in all layers. The results suggest that OECs but not astrocytes contact the BBB in the outer sublamina of the ONL, while in the inner sublamina and in deeper layers the BBB has the typical structure as described in other parts of the brain, comprising astrocyte endfeet. Hence, the BBB in the mammalian brain does not inevitably require the contribution of astrocytes.

2 | MATERIAL AND METHODS

2.1 | Animals

Colonies of NMRI (Naval Medical Research Institute) mice (age: postnatal days 09–12; p09-p12) and PLP-Cre^ERT2 x tdTomato^fl/fl and hGFAP-EGFP_GFEC mice (p28-p42) (Hirrlinger et al., 2005; Leone et al., 2003; Madisen et al., 2010) were obtained from the institutional animal facility at the University of Hamburg. To induce tdTomato expression in PLP-Cre^ERT2 x tdTomato^fl/fl mice, tamoxifen (Carbolution Chemicals GmbH, St.Ingbert, Germany) was dissolved in 8% ethanol/92% Mygliol®812 (Sigma Aldrich, Taufkirchen, Germany) and injected intraperitoneally for three consecutive days (starting p21; 100 mg/kg bodyweight). Only heterozygous PLP-CreERT2 and hGFAP-EGFP mice were used in this study. Animals were analyzed 10–14 days after the first injection. Animal rearing and dissection was performed according to the European Union's and local animal welfare guidelines (GZ G21305/591-00.33; Behörde für Gesundheit und Verbraucherschutz, Hamburg, Germany).

2.2 | Immunohistochemistry

The olfactory bulbs were prepared and kept at room temperature (RT) in 4% formalin in phosphate buffered solution (PBS) containing (in mM): 130 NaCl, 7 Na_2HPO_4, 3 NaH_2PO_4. Afterward 100–150 μm thick sagittal or frontal tissue slices were prepared using a vibratome (VT1000S, Leica, Nussloch, Germany) following 1 hr incubation in blocking solution (10% normal goat serum, 0.5% Triton X-100 in PBS) at RT. Subsequently slices were incubated for 48 hr at 4°C with the primary antibody solution (antibodies were diluted in 1% NGS, 0.05% TritonX100 in PBS). The following antibodies were used: rabbit anti-S100B (1:1,000, Dako), mouse anti-S100B (1:1,000, Santa Cruz Biotechnology, Dallas, TX), rabbit anti-AQP4 (1:1,000, Sigma Aldrich, Taufkirchen, Germany), chicken anti-GFAP (1:1,000, Abcam, Cambridge UK), rat anti-PDGFRβ (1:100, eBioscience, San Diego, CA), chicken anti-GFP (1:500, Abcam), rabbit anti-ZO-1 (1/200, Invitrogen, Carlsbad, CA). Slices were incubated with the following secondary antibodies for 24 hr at 4°C: goat anti-rabbit Alexa 488 (1:1,000 in PBS; Thermo Fisher, Darmstadt, Germany), goat anti-rabbit Alexa 555 (1:1,000 in PBS; Thermo Fisher), goat anti-chicken Alexa 488 (1:1,000 in PBS; Abcam), goat anti-rat Alexa 488 (1:1,000 in PBS, Abcam). Goat anti-mouse secondary antibodies (Alexa 405 and Alexa 555; 1:1,000, Thermo Fisher) were employed to stain blood vessels by the detection of mouse IgGs. Additionally, Hoechst 33342 or DAPI (each 5 μM; Molecular Probes, Eugene, OR) was added to stain nuclei. Slices were mounted on slides using a self-hardening embedding medium (Immu-Mount, Thermo Fisher). Immunohistological stainings were analyzed using a confocal microscope Nikon eC1. Z-Stacks were taken in 100 nm step sizes and 2,048 × 2,048 pixel. Deconvolutions of the z-stacks were established using the Huygens Essential program. Moreover, image z-stacks were projected using an average projection tool in ImageJ and adjusted to contrast and brightness using Adobe Photoshop CS6.

2.3 | Ultrathin section electron microscopy

NMRI mice were transcardially perfused with either 2.4% glutaraldehyde and 2% lanthanum nitrate in HMSS or solely with 2.4% glutaraldehyde in HMSS. The olfactory bulbs were prepared and postfixed in the identical fixative for at least 4 hr. Preparations were stored in cacodylate. The olfactory bulbs were postfixed in 1% OsO_4, following hydration in an ethanol series (50, 70, 96, 100%). To enhance the contrast 70% ethanol was saturated with uranyl acetate. Dehydration was completed in propylene oxide. The preparations were embedded in Araldite (Serva, Heidelberg, Germany). Ultrathin sections were prepared using a FCR Reichert Ultracut ultramicrotome (Leica, Bensheim, Germany), following the mounting on pioloform-coated copper grids, contrasted with lead citrate. The sections were analyzed using an EM10A electron microscope (Carl Zeiss, Oberkochen, Germany).

2.4 | Ca^{2+} imaging and data analysis

In-toto preparations of the olfactory bulb were prepared as described in previous studies (Stavermann et al., 2012; Thyssen et al., 2010). Animals were sacrificed and both olfactory bulbs were removed from the opened head in cooled preparation solution (see below), glued onto small coverslips and stored for 45 min in carbogen-gassed ACSF at 30°C for recovery. Standard artificial cerebrospinal fluid (ACSF) consisted of (in mM): 120 NaCl, 2.5 KCl, 1 $NaH_2PO_4 \times 2H_2O$, 26 $NaHCO_3$, 2.8 D-(+)-glucose, 1 $MgCl_2$, 2 $CaCl_2$. The preparation solution consisted of (in mM) 83 NaCl, 1 $NaH_2PO_4 \times 2H_2O$, 26.2 $NaHCO_3$, 2.5 KCl, 70 saccharose, 20 D-(+)-glucose, 2.5 $MgSO_4 \times 7H_2O$. Both solutions were continuously gassed with carbogen (95% O_2, 5% CO_2) to maintain the pH of 7.4 and to supply oxygen. Whole bulbs were transferred into a recording chamber and fixed with a platinum grid. The preparations were continuously perfused with ACSF (at RT) via a perfusion system. For multi-cell bolus loading a glass pipette with a resistance of ~3 MΩ was filled with 200 μM Fluo-4 AM in ACSF, made from a 4 mM stock solution (dissolved in DMSO and 20% pluronic acid) (Stosiek, Garaschuk, Holthoff, & Konnerth, 2003). The injection pipette was inserted onto the ONL, following the pressure-injection of the Ca^{2+} indicator with 0.7 bar for 30 s into the tissue (PDES-01 AM, npi electronic GmbH, Tamm, Germany). After an incubation of 20 min. Ca^{2+} signals in OECs were detected by the fluorescence of Fluo-4 (excitation: 488 nm, emission: 500–530 nm) using a confocal microscope (eC1, Nikon, Düsseldorf, Germany). Images were acquired at a time rate of one frame every 3–5 s. To analyze Ca^{2+} changes in single cell somata, regions of interest (ROIs) were defined, using Nikon EZ-C1 3.90 FreeViewer software. Cells located in the ONL were defined as OECs (Au et al., 2002; Thyssen et al., 2010). Changes in cytosolic Ca^{2+} were recorded throughout the experiments as relative changes in Fluo-4 fluorescence (ΔF) with respect to the resting fluorescence, which was normalized to 100%.

## 2.5 | Visualization of blood vessels and glucose uptake

After bulk loading with Fluo-4 AM, a micropipette with a resistance of 7–8 MΩ (when filled with ACSF) was loaded with 1 μM sulforhodamine 101 (SR101; Santa Cruz Biotechnology) diluted in ACSF and inserted into a blood vessel located in the ONL. SR101 was pressure injected (0.1 bar, 30 s) into the blood vessel, resulting in an immediate labeling of the blood vessel network throughout the olfactory bulb (Figure S1). SR101 was excited by a helium-neon laser (excitation 543 nm, emission: 553–618 nm) of the confocal microscope. Vasoconstriction was measured as the decrease of the SR101 fluorescence in a region of interest, covering the entire cross sections of a blood vessel segment of ~10–20 μm length. The fluorescent non-hydrolyzable glucose analog, 6-(N-(7-nitrobenz-2-oxa-1,3-diazol-4-yl) amino)-6-deoxyglucose (6-NBDG, 100 μM in ACSF; Thermo Fisher) was injected into the blood vessels similar to SR101 to visualize glucose uptake into glial cells. 6-NBDG was excited by a 488-nm argon laser.

3 | RESULTS

3.1 | Glial distribution in the ONL

We aimed to analyze the glial organization of the BBB in the ONL using immunohistology. OECs are strongly S100B-positive, whereas astrocytes, in particular in neonatal brains, show less immunoreactivity against S100B (Au et al., 2002; Raponi et al., 2007; Thyssen et al., 2013) (Figure 1a,b). Astrocytes in the GL, however, express high amounts of GFAP, whereas OECs are GFAP-negative (Au et al., 2002; Doengi, Deitmer, & Lohr, 2008; Doucette, 1984; Thyssen et al., 2013) (Figure 1a–e). We did not perfuse the blood vessel system during fixation, hence blood vessels contain endogenous antibodies including IgG. Blood vessels were detected by goat anti-mouse IgG antibodies labeled with Alexa Fluor 405, enabling the visualization of the dense vascular network of the olfactory bulb (Doengi et al., 2009). (Figure 1b–e). S100B-positive OECs are exclusively located in the ONL. In the outer ONL, S100B-positive OEC somata and processes are in close contact to blood vessels (Figure 1d). GFAP-positive somata of astrocytes are located throughout all layers of the olfactory bulb, except the ONL. However, few GFAP-positive astrocytic processes project into the inner ONL, intermingling with blood vessels (Au et al., 2002; Bailey & Shipley, 1993; Petzold, Albeanu, Sato, & Murthy, 2008; Rieger, Deitmer, & Lohr, 2007; Figure 1e).

Although S100B expression is lower in OB astrocytes compared to OECs in mice of an age up to 2 weeks, mature astrocytes contain similar amounts of S100B as OECs, suggesting that S100B might not be an ideal marker to distinguish between OECs and astrocytes (Beiersdorfer, Scheller, Kirchhoff, & Lohr, 2019). Therefore, we took advantage of PLP-Cre^{ERT2} x tdTomato$^{fl/fl}$ x hGFAP-EGFP$_{GFEC}$ mice, in
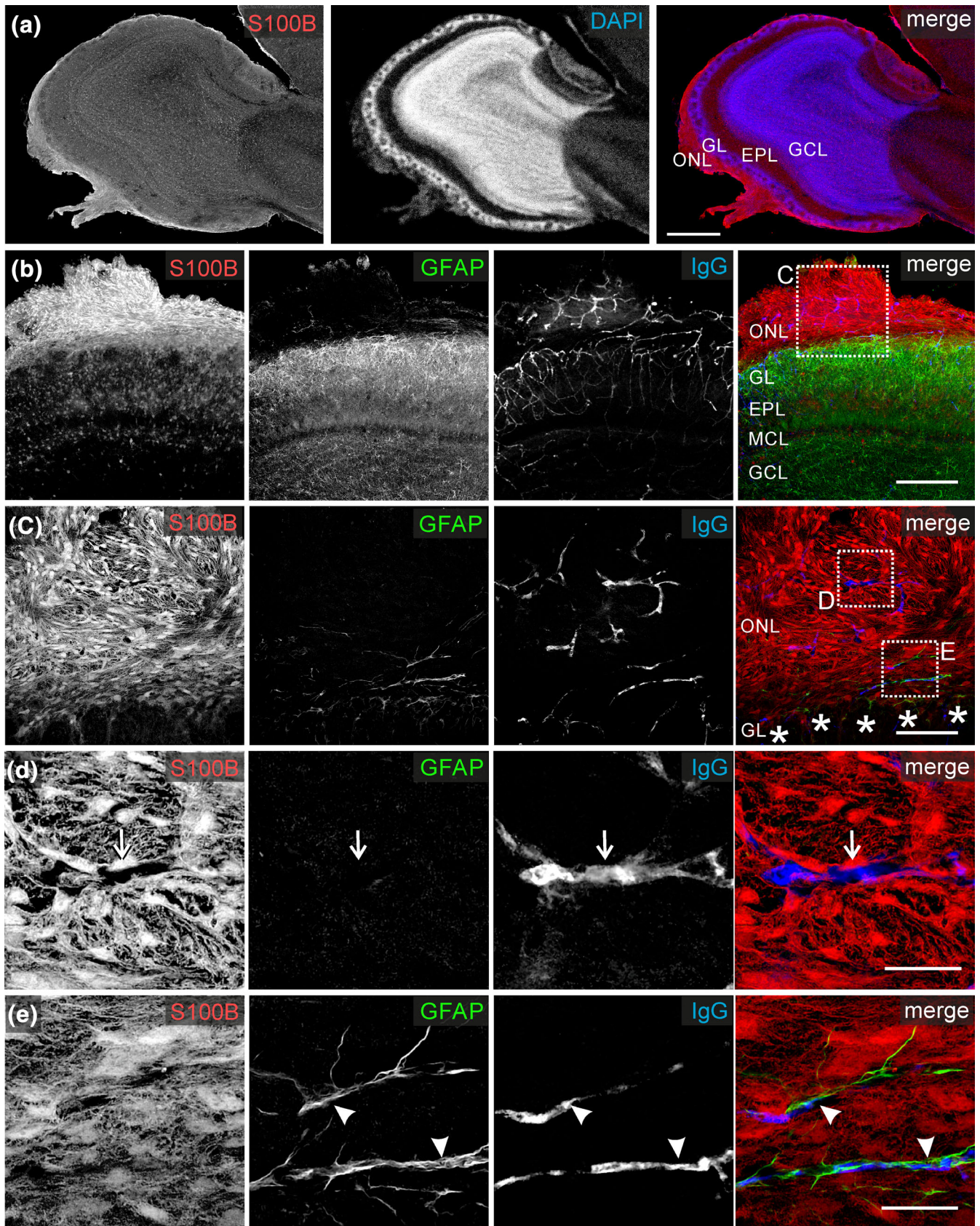
FIGURE 1 Legend on next page.

which OECs express tdTomato controlled by the PLP promotor and astrocytes express EGFP controlled by the hGFAP promotor (Hirrlinger et al., 2005; Leone et al., 2003; Madisen et al., 2010). The cytosolic expression of the fluorescent reporters in OECs and astrocytes enabled the visualization of the entire cell, in contrast to, for example, GFAP antibody staining that only labels major cell processes. tdTomato-expressing OECs are located in the entire ONL (Figure 2a). Oligodendrocytes are located in the GL, but not the ONL which only contains unmyelinated axons (Dickinson et al., 1997). Hence, tdTomato-expressing cells located in the GL are addressed as oligodendrocytes. EGFP-expressing astrocytes are present in the GL and extend processes in the inner ONL (Beiersdorfer et al., 2019) (Figure 2a). In particular, blood vessels are ensheathed by GFP-expressing astrocytes in the inner ONL, whereas tdTomato-expressing OECs contact the same blood vessel in the outer ONL (Figure 2b). Our results suggest that OECs might contact the BBB in the outer ONL, whereas in the inner ONL and deeper layers, blood vessels are surrounded by astrocytes. To verify that in the outer ONL OECs tightly enwrap blood vessels, we performed ultrastructural studies (Figure 2c,d). EM images showed the cellular elements of the BBB in the ONL of a mouse at an age of 9 days (P9). ECs form the blood vessel wall and are surrounded by a thin (<50 nm) basal lamina. Moreover, OECs surround the blood vessels with their processes as shown by immunohistochemistry. Similar results have been found in juvenile mice (P21; Figure S2).

## 3.2 | Astrocytic endfeet are part of the BBB in the inner ONL

AQP4 is a member of the water-channel protein family of aquaporins and is supposed to be exclusively expressed in astrocyte endfeet in the brain (Nielsen et al., 1997; Rash & Yasumura, 1999; Simard, Arcuino, Takano, Liu, & Nedergaard, 2003; Wolburg, Wolburg-Buchholz, Fallier-Becker, Noell, & Mack, 2011). Located at the border between blood vessels and the neuropil, AQP4 channels provide osmotic balance and homeostasis within the CNS (Nico et al., 2001). In the GL of the OB, a dense network of AQP4-positive astrocyte endfeet has been investigated, while the literature lacks information about AQP4 in the ONL (Petzold et al., 2008). We aimed to analyze the expression of AQP4 in the ONL and its contribution to the BBB. In addition, we stained for GFAP to identify astrocytes. The vasculature was visualized by the detection of mouse IgGs. AQP4 is highly expressed within the GL, however, AQP4 immunoreactivity was not restricted to astrocyte endfeet surrounding blood vessels, but appears to label most of the astrocyte structures (Figure 3a; Petzold et al., 2008). AQP4 expression can also be detected in the inner ONL around blood vessels, on astroglial endfeet (Figure 3b). In addition, AQP4-positive structures are frequently found in the outer ONL, neither associated with the vasculature nor contributing to GFAP-positive astrocytes (Figure 3c). In the entire ONL, immunoreactivity of AQP4 does not co-localize with tdTomato-expressing OECs in PLP-Cre[ERT2] x tdTomato^{fl/fl} mice (Figure 3d).

3.3 | Pericytes are part of the BBB in the ONL

As a cellular component of the BBB, pericytes fulfill a whole repertoire of functions, including stabilization of the vasculature, angiogenesis, macrophage-like function, and regulation of endothelial cell proliferation (Hamilton, Attwell, & Hall, 2010; Hirschi & D'Amore, 1996; Lai & Kuo, 2005). In in-vivo studies of the ONL, Chaigneau, Oheim, Audinat, and Charpak (2003) did not find any capillaries, but arterioles as defined by the vessel diameter (<6 μm for capillaries). In the GL, on the other hand, a dense capillary network was analyzed in that study. In contrast, Halasz, Ljungdahl, and Hokfelt (1979) reported capillaries in EM studies of the ONL. We investigated the distribution of pericytes in the ONL by immunohistochemistry using anti-PDGFRβ (platelet-derived growth factor receptor β), a marker for pericytes (Armulik, Mae, & Betsholtz, 2011; Attwell, Mishra, Hall, O'Farrell, & Dalkara, 2016; Winkler et al., 2018; Winkler, Bell, & Zlokovic, 2010). Our results show PDGFRβ-positive pericytes located around blood vessels in the ONL and GL (Figure 4a). Co-staining with anti-S100B showed an envelope of OECs around PDGFRβ-positive pericytes in the outer ONL (Figure 4b,c). In the inner ONL and the GL, in contrast, PDGFRβ-positive pericytes were enwrapped by AQP4-positive astrocyte processes (Figure 4d,e). It should be emphasized that there are no ideal markers exclusively labeling pericytes independent of area, developmental stage, or experimental conditions (Armulik et al., 2011; Gerhardt & Betsholtz, 2003). Different studies suggest PDGFRβ expression in developing vascular smooth muscles cells (vSMC) restricted to arterioles, as well as endothelial cells and neurons (Hellstroem, Kalen, Lindahl, Abramsson, & Betsholtz, 1999; Lindahl et al., 1997; Smits et al., 1991). However, ultrastructural analyses verified the existence of pericytes around blood vessels in the ONL and showed that the cross section of the blood vessel walls were built by

FIGURE 1 Distribution of glial cells and blood vessels in the olfactory nerve layer (ONL) of neonatal mice. (a) Overview of the olfactory bulb. Olfactory ensheathing cells (OECs) in the olfactory nerve layer (ONL) and astrocytes in the glomerular layer (GL), external plexiform layer (EPL), and granule cell layer (GCL) are S100B-positive (red). Nuclei are stained with DAPI. Scale bar: 500 μm. (b) At higher magnification, OECs in the ONL are strongly S100B-positive (red), whereas astrocytes in the GL, EPL, and GCL show weaker expression of S100B. GFAP-positive astrocytes are localized throughout the GL, EPL, and GCL (green). The vascular network, visualized by immunostaining of mouse IgGs (blue), extends throughout all layers of the olfactory bulb. Scale bar: 200 μm. (c) Magnified detail from (b). Asterisks indicate glomeruli. Scale bar: 50 μm. (d) Magnified detail of the outer ONL, as indicated in (c). S100B-positive OECs are closely associated with blood vessels in the outer ONL, lacking GFAP-positive structures (arrows). Scale bar: 15 μm (e) Magnified detail of the inner ONL as indicated in (c). GFAP-positive astrocytes are closely associated with blood vessels (arrowheads). Scale bar: 15 μm
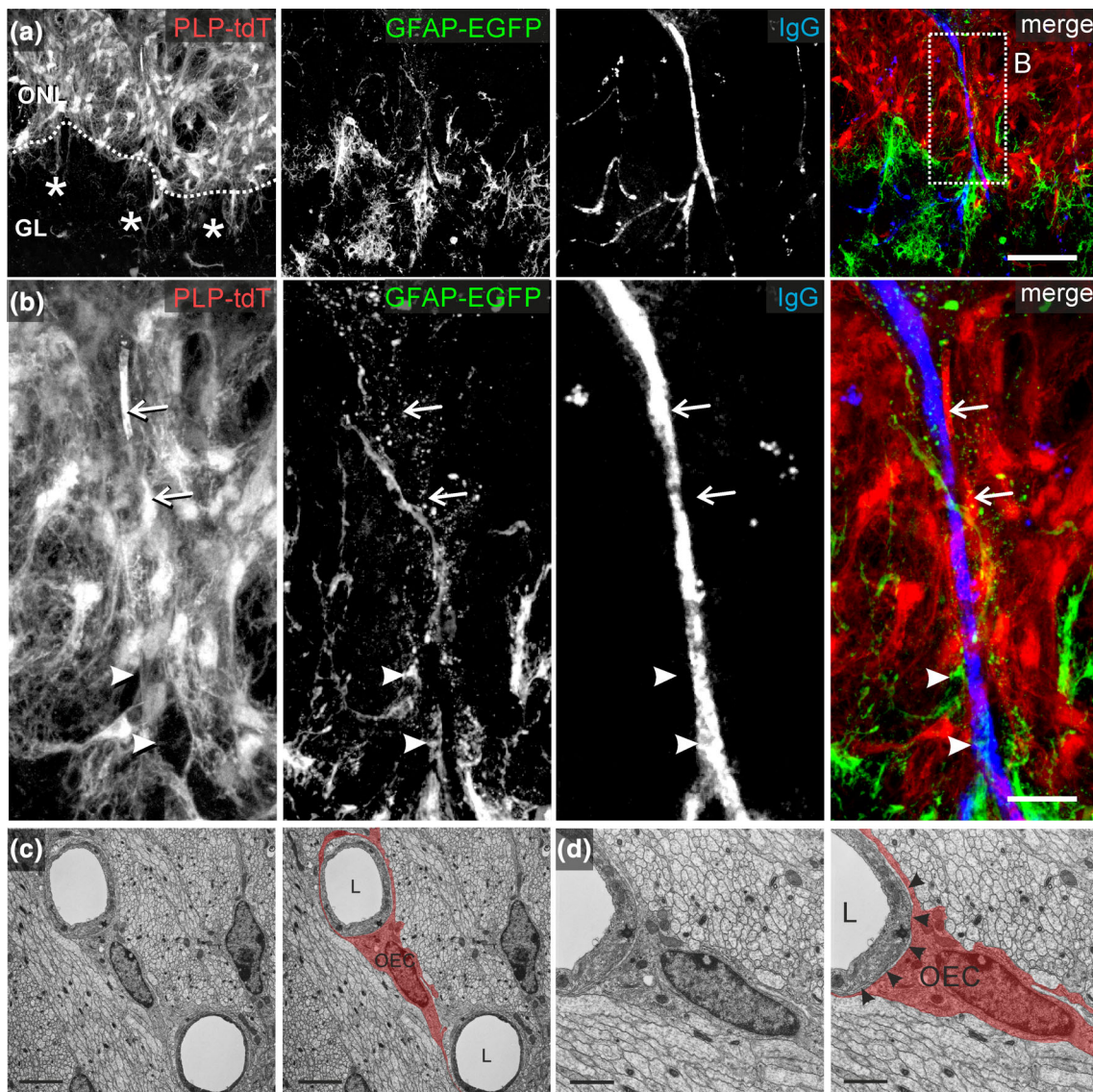
FIGURE 2 Organization of the blood brain barrier (BBB) in PLP-Cre^ERT2/tdT x GFAP-EGFP mice (a) tdTomato-expressing olfactory ensheathing cells (OECs; red) are located in the olfactory nerve layer (ONL). Cell bodies of EGFP-expressing astrocytes (green) are located in the glomerular layer (GL). Immunostaining against mouse IgG outlines the vascular network (blue) in the GL and ONL. One blood vessel crosses the entire ONL and finally enters one glomerulus. Scale bar: 50 μm (b) Magnified detail as indicated in (a). EGFP-expressing astrocytes are tightly associated with the blood vessel located in the inner ONL (arrows), while tdTomato-expressing OECs are in close contact to the same blood vessel as it proceeds in the outer ONL (arrowhead). Scale bar: 20 μm (c) Electron micrograph of the BBB in the ONL. Blood vessels (lumen, L) located in the ONL are ensheathed by OECs. One OEC is highlighted in red in the right panel. Scale bar: 2 μm. (d) Magnified detail from (c). OEC processes are separated from the blood vessel by a thin layer of basal lamina (arrowheads). Scale bar: 1 μm

one to two endothelial cells, typical for capillaries (Joost et al., 2019; Figure 4f,g and Figure S2). Hence, our results demonstrate pericytes associated with capillaries in the ONL.

3.4 | Selective permeability of the blood brain barrier in the ONL

One function of the BBB is a selectivity filter for molecular exchange between brain tissue and blood; For example, entry of noxious substances into the brain parenchyma is restricted, whereas nutrients are

actively transported into brain tissue. Glucose, the main source of energy in the brain, is transported across endothelial cells via glucose transporters 1 (GLUT-1), released into the extracellular space, where it is taken up by astrocytes, metabolized into lactate and provided to neurons (Barros & Deitmer, 2010; Simpson, Carruthers, & Vannucci, 2007; Zhao et al., 2015). 2-deoxyglucose autoradiography studies have shown high glucose consumption in the ONL (Benson et al., 1985; Sharp et al., 1977). Since our previous results showed that OECs ensheath not only OSN axons, but also blood vessels in the ONL and thereby might link both structures together (Thyssen et al., 2010), we asked whether OECs might take up glucose from the
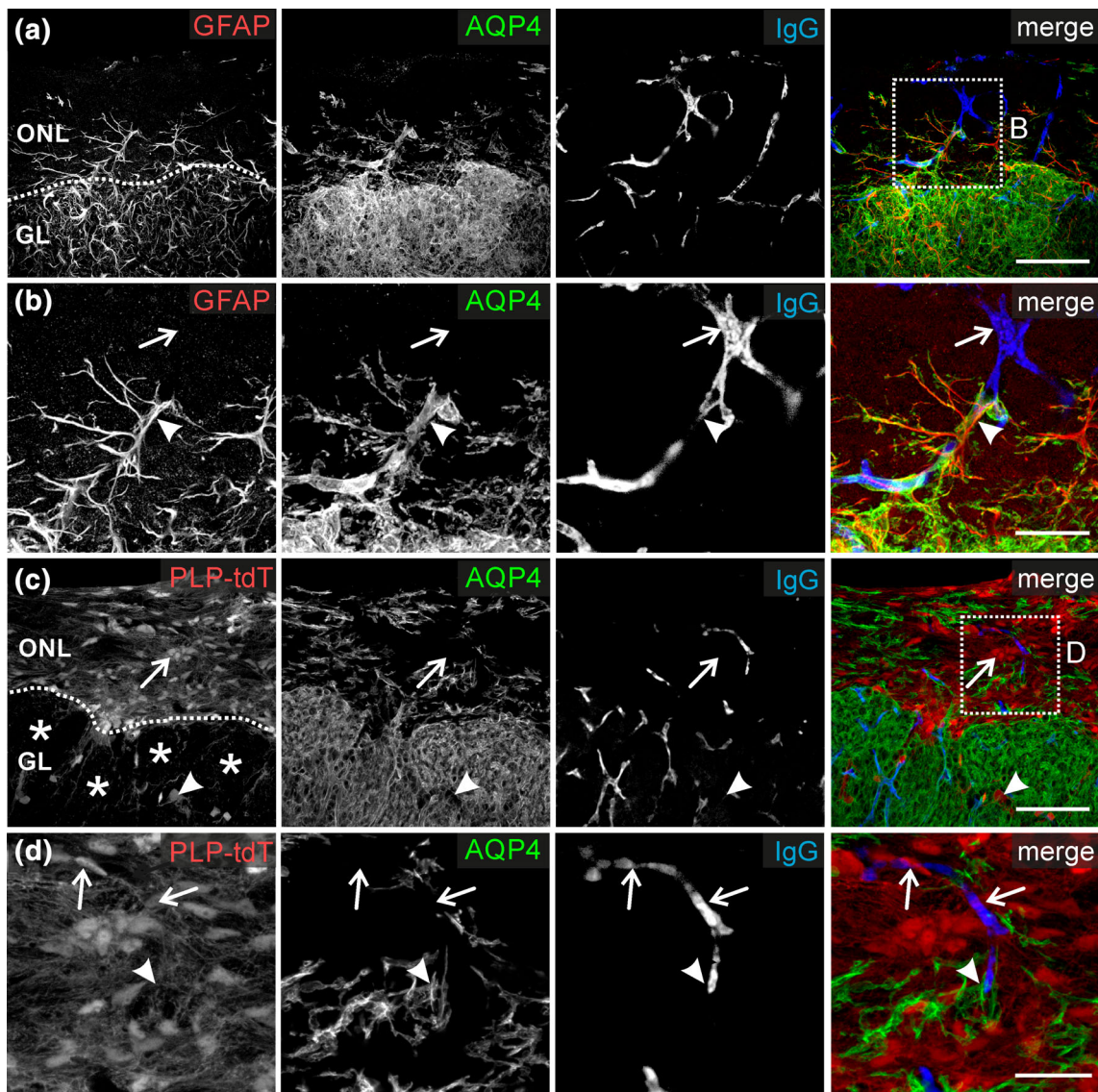
FIGURE 3 Astrocytic endfeet surround blood vessels in the inner olfactory nerve layer (ONL). (a) GFAP-positive astrocytes (red) co-localize with AQP4 immunoreactivity (green). Blood vessels are immunostained against mouse IgG (blue). Scale bar: 50 μm. (b) Magnified detail from (a). GFAP and AQP4 immunostaining colocalize in the inner ONL. One blood vessel extends from the glomerular layer (GL) to the ONL and is ensheathed by AQP4- and GFAP-positive astrocytic endfeet in the inner ONL (arrowhead), while it is devoid of AQP4- and GFAP-expressing glial processes in the outer ONL (arrows). Scale bar: 20 μm. (c) PLP-driven tdTomato expression (red) in olfactory ensheathing cells (OECs) in the ONL (arrow) and oligodendrocytes in the GL (arrowhead). Scale bar: 50 μm. (d) Magnified detail from (c). Blood vessels located in the GL and inner ONL are ensheathed by AQP4-positive astrocytic endfeet (arrowhead), whereas tdTomato-expressing OECs are associated with blood vessels located in the outer ONL (arrow). Scale bar: 20 μm

perivascular space to provide energy to OSN axons. To monitor glucose uptake into glial cells in previous studies, the fluorescent non-hydrolyzable glucose analog 6-NBDG has been used in the cerebellum and hippocampus in situ as well as in the somatosensory cortex in vivo (Barros et al., 2009; Chuquet, Quilichini, Nimchinsky, & Buzsaki, 2010; Jakoby et al., 2014). We used 6-NBDG to visualize glucose uptake in olfactory bulb in-toto preparations of PLP-Cre[ERT2] x tdTomato^{fl/fl} mice, enabling identification of OECs by tdTomato expression. Under optical control, 6-NBDG was pressure-injected into a large blood vessel located in the lateral ONL, resulting in loading of 6-NBDG into the blood vessel network (Figure 5a). OECs located

close to a 6-NBDG-filled blood vessel, but at least 100 μm apart from the injection site, were analyzed. tdTomato-positive OECs adjacent to blood vessels were labeled by 6-NBDG within 3–5 min after injection of 6-NBDG into blood vessels, indicating glucose uptake by OECs from the extracellular space close to blood vessels (Figure 5a). Interestingly, OECs which were not directly associated with blood vessels, but near 6-NBDG-loaded perivascular OECs, were also labeled by 6-NBDG, confirming previous results of gap junction coupling between OECs (Piantanida et al., 2019; Rela, Bordey, & Greer, 2010). We did not find apparent labeling of axon bundles by 6-NBDG, suggesting that there is little uptake of glucose by axons in the ONL.
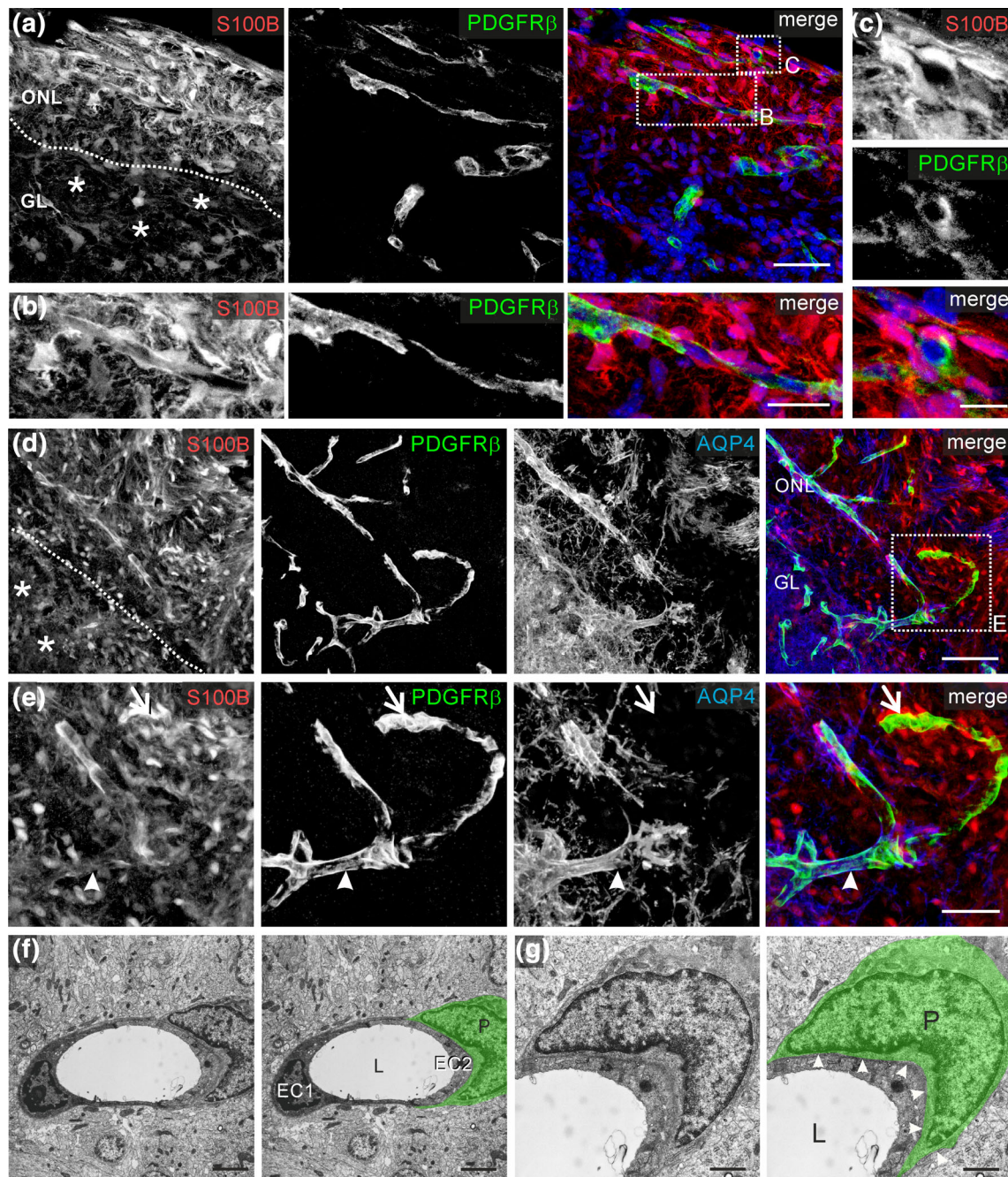
FIGURE 4 Pericytes are part of the blood brain barrier (BBB) in the inner and outer olfactory nerve layer (ONL). (a) S100B (red) and PDGFRβ immunoreactivity (green) in the ONL and the glomerular layer (GL). Nuclei were counterstained with Hoechst in the merged image (blue). Scale bar: 50 μm. (b) The magnified detail from (a) depicts a longitudinal section of a blood vessel tightly ensheathed by PDGFRβ-positive pericytes (green) and S100B-positive olfactory ensheathing cells (OECs; red) in the ONL. Scale bar: 25 μm. (c) Magnified details from (a), showing a cross section of a blood vessel ensheathed by PDGFRβ-positive pericytes (green) and S100B-positive OECs (red) in the ONL. Scale bar: 12.5 μm. (d) S100B (red), PDFGRβ (green) and AQP4 (blue) immunoreactivity in the GL and ONL (green). Scale bar: 50 μm. (e) Magnified detail of the ONL as indicated in (d). A blood vessel is ensheathed by PDGFRβ-positive pericytes and AQP4-positive astrocytic endfeet in the inner ONL (arrowhead), but lacks AQP4-positive ensheathment in the outer ONL (arrow). Scale bar: 25 μm. (f) Electron micrograph of the BBB in the ONL. A pericyte (green outline in right panel) is directly located on a blood vessel composed by two endothelial cells (EC1 and EC2). L, lumen. Scale bar: 2 μm. (g) At higher magnification, the basal lamina is visible (arrowheads). Scale bar: 1 μm

Endothelial cells are connected by tight junctions, which maintain the barrier function by controlling paracellular diffusion of substances from the blood stream into the CNS (Abbott et al., 2010). To investigate the presence of the cytoplasmic tight junction protein, ZO-1 (zonula occludens 1) at the BBB in the ONL, we performed immunofluorescent staining in NMRI mice (Wolburg et al., 2008; Wolburg & Lippoldt, 2002; Figure 5b). The vasculature was visualized by the detection of mouse IgGs. Blood vessels located in the entire ONL

FIGURE 5 Selective permeability of the blood brain barrier (BBB) in the olfactory nerve layer (ONL). (a) PLP promotor-driven tdTomato expression (red) in the ONL in an in-toto preparation. The fluorescent glucose analog 6-NBDG (green) was pressure-injected into a blood vessel and spread within the vascular network. tdTomato-positive OECs located close to the blood vessels took up 6-NBDG (arrowheads), while distant olfactory ensheathing cells (OECs) were not labeled by 6-NBDG (arrows). Scale bar: 5 μm. (b) ZO-1 immunoreactivity (green) in the ONL and the GL. Nuclei were counterstained with Hoechst (blue, in merged image) and blood vessels were immunostained against mouse IgG (red). Blood vessels in the ONL are ensheathed by ZO-1-positive tight junctions. Scale bar: 50 μm. (c) Lanthanum nitrate was transcardically perfused before fixation and visualized by the black precipitation in electron micrographs. Scale bar: 1 μm. (d) Magnified detail from (c). Endothelial tight junctions limited diffusion of lanthanum nitrate out of the blood vessel (arrow). Scale bar: 0.5 μm
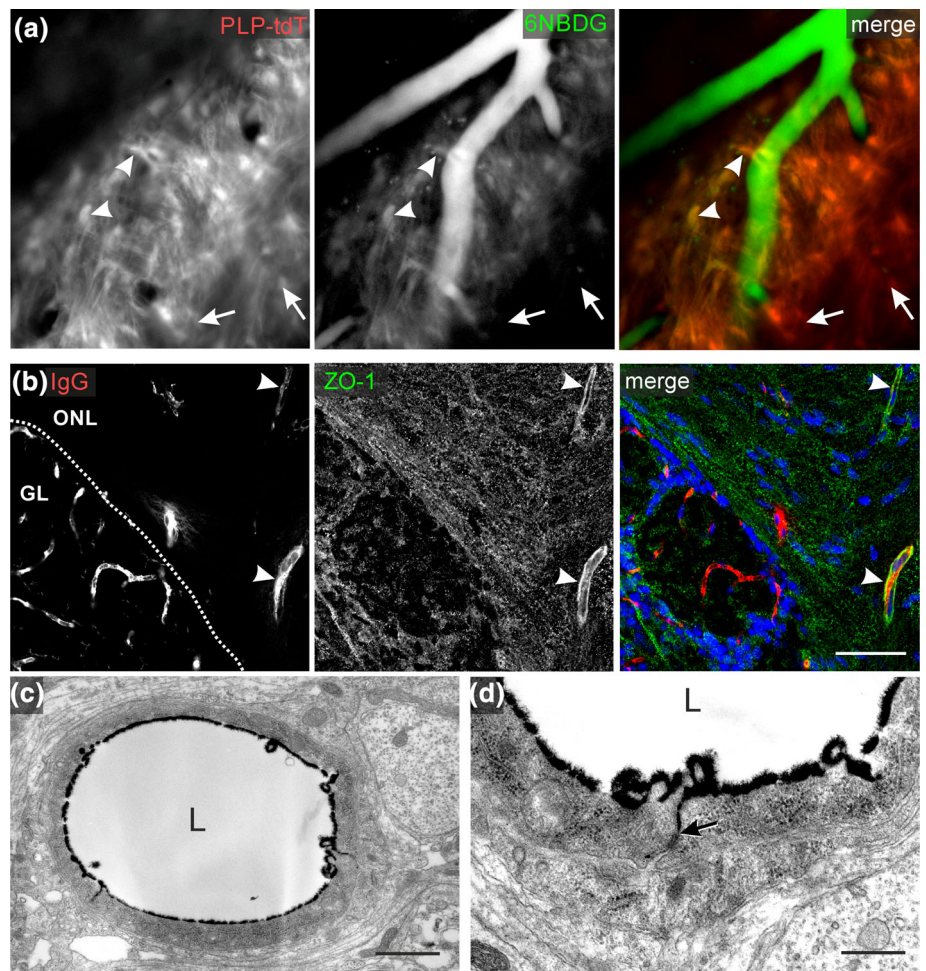
showed immunoreactivity against ZO-1, substantiating the presence of tight junctions between adjacent endothelial cells at the BBB in the ONL. Interestingly, blood vessels in the GL often showed less ZO-1 immunoreactivity. To analyze the impermeability for noxious substances of the BBB in the ONL, we perfused NMRI mice transcardically with 2% lanthanum nitrate in glutaraldehyde. In electron micrographs, lanthanum nitrate is detected as a black precipitate (Figure 5c). In case of leakage of the BBB, lanthanum nitrate diffused across the inter-endothelial cleft into the sub-endothelial space, as it has been shown for blood vessels in the olfactory lamina propria (Wolburg et al., 2008). In the ONL, in contrast, lanthanum diffused only a small distance between the endothelial cells, until further diffusion was prevented by tight junctions, indicating an intact and impermeable BBB (Figure 5(d); Figure S2).

3.5 | Ca^{2+} signaling in OECs triggers vasoresponses in the outer ONL

The ONL harbors at least two subpopulations of OECs differing in the expression pattern of marker proteins, physiological properties and their localization in the inner and outer ONL, respectively (Au et al., 2002; Honore et al., 2012; Rela et al., 2010; Rela, Piantanida,

Bordey, & Greer, 2015; Thyssen et al., 2013). Release of glutamate and ATP from OSN axons initiates Ca^{2+} responses in OECs in the outer ONL, but not in OECs of the inner ONL, which instead propagate spontaneous Ca^{2+} waves that do not include OECs of the outer nerve layer (Stavermann et al., 2015; Thyssen et al., 2013). Since our results demonstrate differences in the morphological relationship of blood vessels and OECs between the outer and inner ONL, we asked whether both subpopulations of OECs differ in their ability to initiate vasoresponses. Therefore, we performed Ca^{2+} imaging experiments using in-toto preparations of the olfactory bulb in which blood vessels were visualized by SR101 injection. The Ca^{2+} indicator Fluo-4 AM was pressure-injected into the ONL, resulting in labeling of OECs with Fluo-4. Ca^{2+} transients in OECs of the outer ONL were induced by focal pressure application of the mGluR agonist DHPG (100 μM) onto the ONL (Thyssen et al., 2010). DHPG induced Ca^{2+} responses in OECs of the outer ONL with an amplitude of 127.1 ± 10.1% ΔF (n = 35), followed by a decrease in SR101 fluorescence by 25.3 ± 3.3% (n = 18) in associated blood vessels, indicating vasoconstriction (see ROI 2 in Figure 6a,b and Movie S1). Adjacent branches of the capillaries responded with a delay (see ROIs 3 and 4), whereas no vasoresponses could be observed in distal capillaries and upstream arterioles (see ROIs 5 and 6). Spontaneous Ca^{2+} signals occurring during Ca^{2+} wave propagation in OECs of the inner sublamina

(a) Outer nerve layer
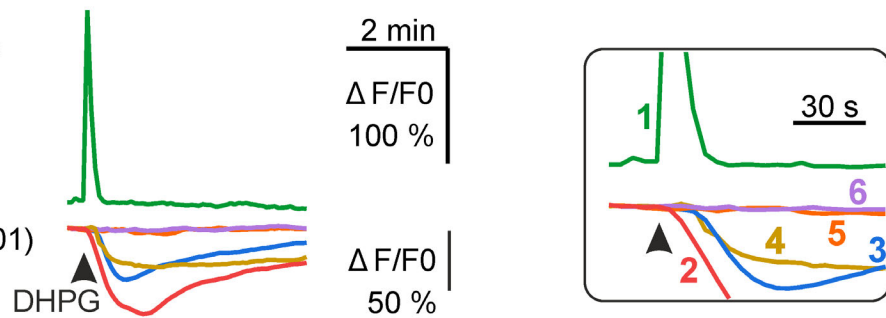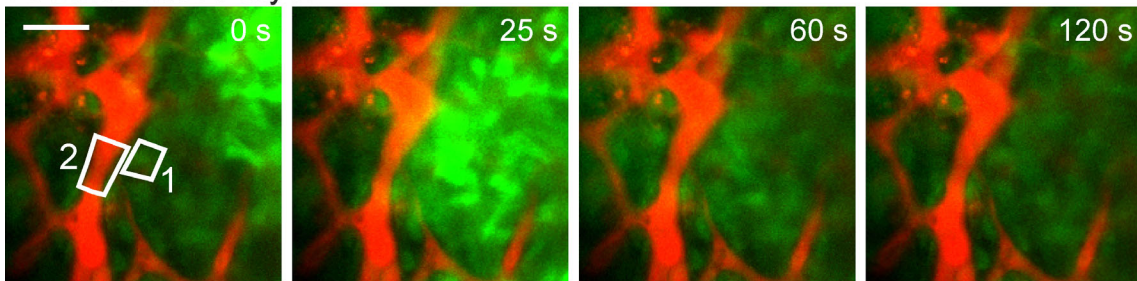

(b)
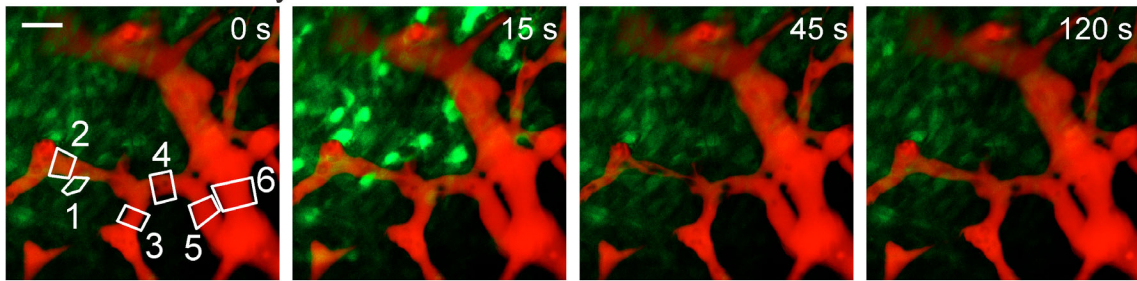
(c) Inner nerve layer

(d)
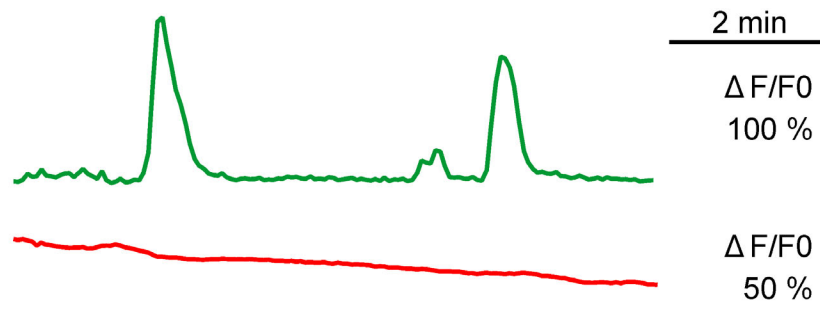
FIGURE 6 Ca^{2+} signaling in olfactory ensheathing cells (OECs) mediates vasoconstriction in the outer olfactory nerve layer (ONL). (a) Blood vessels located in the outer ONL are injected with SR101 (red) and associated OECs are loaded with Fluo-4 (green). Image sequence of DHPG-induced Ca^{2+} transients in OECs, followed by a decrease in SR101 fluorescence, indicating vasoconstriction. DHPG was pressure-applied from a micropipette located at the left border of the image. Scale bar: 20 μm. (b) ROI1 (as indicated in (a)) represents an OEC selected for analysis. SR101 fluorescence was measured in ROI2 to 6 (as indicated in (a)). The inset represents the time course of Ca^{2+} signaling in OECs and the following vasoconstriction in different sections of the vascular tree from higher-order capillaries (ROI2-4), primary capillary (ROI 5), and upstream arteriole (ROI 6; see also Movie S1). The capillary directly adjacent to OECs responding to DHPG stimulation responded first and with the strongest constriction (ROI2), followed by adjoining capillary sections (ROIs 3 and 4). No changes in vascular tone could be observed in distant capillaries and the upstream arteriole (ROIs 5 and 6). (c) Image sequence of a spontaneous Ca^{2+} wave propagating in OECs of the inner ONL. Scale bar: 10 μm. (d) ROI1 represents the OEC selected for analysis in (c). SR101 fluorescence was measured in ROI2 as indicated in (c). Spontaneous Ca^{2+} wave propagation in OECs (represented by ROI1) is not followed by a change in blood vessel diameter (ROI2; see also Movie S2)

(Stavermann et al., 2015), in contrast, did not trigger vasoconstriction of associated blood vessels (Figure 6c,d; Movie S2).

The results show that Ca^{2+} responses in OECs of the outer sublamina are capable to trigger local changes in blood vessel diameter. In the inner ONL, on the other hand, vasoresponses were not evoked by Ca^{2+} signals in OECs, supporting the notion that there are functional differences between the two subpopulation of OECs regarding the gliovascular interface.

4 | DISCUSSION

In the present study, we investigated the cellular organization of the BBB in the ONL, using electron microscopy and immunofluorescence staining. Our results showed that in the outer sublamina of the ONL, S100B-, and PLP-tdTomato-positive OECs were closely associated with the vasculature, whereas GFAP- and AQP4-positive astrocyte processes were sparse and not joint with blood vessels. In contrast, astrocytic endfeet in the inner sublamina of the ONL enwrapped blood vessels abundantly, indicating that there are cellular differences in the organization of the BBB within the two sublaminae of the ONL (Figure 7).

4.1 | OECs and astrocytes are part of the BBB at the CNS-PNS transitional zone

The ONL consists of incoming axons of olfactory sensory neurons and OECs, which support growth and guidance of axons from the
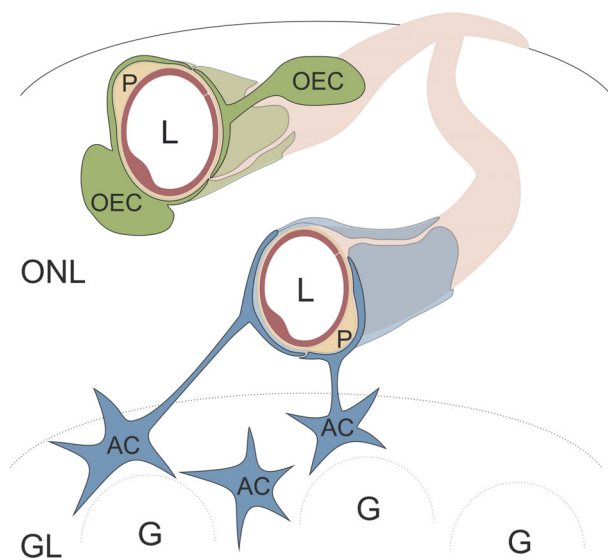
FIGURE 7 Blood brain barrier in the mouse olfactory nerve layer. Capillaries in the outer sublamina of the olfactory nerve layer (ONL) are covered by pericytes (P) and processes of olfactory ensheathing cells (OECs). In the inner sublamina of the ONL, capillaries are covered by pericytes and endfeet of astrocytes (AC), the somata of which are located in the glomerular layer (GL) comprising glomeruli (G). L, lumen of capillary. Illustration by SciGraphics

periphery into the CNS (Doucette, 1990, 1991). Therefore, the ONL represents the CNS-PNS transitional zone, in which the exact borders of CNS and PNS are still under debate (Barnett & Riddell, 2004; Doucette, 1991; Windus et al., 2010). The glia limitans covers the CNS and controls the diffusion of substances into the CNS in combination with the BBB. Recently, Nazareth et al. (2019) have suggested that the glia limitans consists of astrocytes alone, thus at least the outer sublamina of the ONL remains PNS, since astrocytes are absent in the outer ONL (Au et al., 2002; Doucette, 1991). However, the blood nerve barrier (BNB), which is the counterpart to the BBB in the PNS, significantly differs in the cellular organization by lacking a glial compartment (Kanda, 2013). Here, we show that in the outer sublamina of the ONL, S100B-, and PLP-tdtomato positive OECs are in close contact to the vasculature, whereas in the inner sublamina, GFAP- and AQP4-positive astrocytes are part of the BBB (Figures 1 and 2). Similar results were obtained in an ultrastructural study in macaques, showing the association of OECs with local blood vessels (Herrera, Casas, Bates, & Guest, 2005). In contrast, blood vessels of a larger diameter that penetrate the entire ONL (penetrating arterioles) are intensely covered by astrocytes (Doengi et al., 2009; Petzold et al., 2008). Our results suggest that the vasculature in both sublaminae of the ONL is associated with glial cells, in contrast to the BNB in the PNS. OECs originate from the neural crest, share Schwann cell properties and are therefore considered peripheral glial cells (Barraud et al., 2010; Doucette, 1991; Nazareth et al., 2019). However, OECs are also gap junction-coupled to astrocytes that project into the ONL, forming one functional unit (Beiersdorfer et al., 2019). In addition, OECs in the ONL contribute to the glial limitans and the BBB, considering the entire ONL being part of the CNS (Boyd, Skihar, Kawaja, & Doucette, 2003; Doucette, 1991; Herrera et al., 2005; Windus et al., 2010). Furthermore, the BBB and the BNB differ in their permeability properties in means of lanthanum diffusion. Our results show that the vasculature in the ONL is impermeable for lanthanum, a hallmark for the BBB, in contrast to the BNB in the sural nerve and the olfactory lamina propria (MacKenzie, Ghabriel, & Allt, 1987; Wolburg et al., 2008). Taken together, OECs share properties of peripheral and central glial cells, resulting in blurring of the PNS-CNS transitional zone in the ONL and thereby enabling the entry of axons through the olfactory nerve into the brain, a process that is suppressed in other parts of the CNS (Smith, Falone, & Frank, 2012).

4.2 | OECs mediate neurovascular and neurometabolic coupling in the outer ONL

Neuronal activity mediates Ca^{2+} transients in astrocytes, initiating the production and release of vasoactive substances, such as arachidonic acid and prostaglandins, causing a change in arteriole diameter (Filosa et al., 2004; Gordon et al., 2007; Mulligan & MacVicar, 2004; Zonta et al., 2003). In the olfactory bulb, odor stimulation evoked Ca^{2+} transients in perivascular astrocytic endfeet resulting in vasodilatation of arterioles of the inner ONL in vivo (Petzold et al., 2008). We show that ectopic release of glutamate and ATP by OSN axons induced

Ca^{2+} responses in OECs of the outer ONL, resulting in subsequent vasoconstrictions of neighboring blood vessels (Thyssen et al., 2010; Figure 6a,b), while spread of Ca^{2+} waves in OECs of the inner ONL did not influence blood vessel diameter (Figure 6c,d). These findings are in accordance to our histological data, showing that in the outer sublamina, OECs are closely associated with blood vessels, whereas in the inner ONL the vasculature is devoid of OECs but enwrapped by astrocyte endfeet. The results indicate that the two subpopulations of OECs in the inner and outer sublamina not only differ in the presumed interaction with regrowing axons but also in their interaction with the vasculature. In the mouse olfactory bulb, odor stimulation results in dilation of capillaries in the vicinity of glomeruli with odor-dependent synaptic activity; however, capillary dilation was preceded by dilation of up-stream arterioles more than 100 μm apart located in the external and mitral cell layer (Rungta, Chaigneau, Osmanski, & Charpak, 2018). The dilation, possibly mediated by potassium-dependent back-propagating hyperpolarization along the endothelium, was widespread and comprised the entire tree of arteriole, first and higher order capillaries (Longden, Hill-Eubanks, & Nelson, 2016; Longden & Nelson, 2015; Rungta et al., 2018). On the contrary, we showed local constriction of capillaries triggered by Ca^{2+} transients in OECs without previous vasoresponses of upstream capillaries and arterioles (Figure 6a,b; Thyssen et al., 2010). Local constriction of capillaries points to contractility of pericytes, which are present in the ONL (Figure 3). However, it is yet unclear whether pericytes in the brain are able to actively contract (Alarcon-Martinez et al., 2018; Hall et al., 2014; Hill et al., 2015; Vanlandewijck & Betsholtz, 2018). Retrograde hyperpolarization of upstream arterioles, as described above, is caused by accumulation of extracellular potassium after neuronal activity, which activates inward-rectifier K^+ channels producing a fast hyperpolarization of the endothelium (Longden et al., 2017). However, in our experimental conditions, neuronal activity and the subsequent enrichment of external K^+ is lacking, which might account for differences between our study and Rungta et al. (2018). In summary, the present and previous studies show that the mechanism that links neuronal activity to hyperemia is complex and OECs should be included in the models of neurovascular coupling in the olfactory bulb, although future experiments have to unravel the definite role OECs and possible intermediates play therein.

Neuronal information processing is a highly energy-consuming mechanism. To meet those needs, transport of nutrients across the BBB is essential. 2-deoxyglucose studies show high energy consumption in the ONL, an area that lacks cell bodies of astrocytes that classically provide metabolic support to neurons (Giaume, Koulakoff, Roux, Holcman, & Rouach, 2010; Sharp et al., 1977). Our results demonstrate that axon-associated OECs are in close contact to the vasculature, thereby adopting the ideal position to supply metabolites to axons. Additionally, OECs exhibit the ability to take up glucose from the perivascular space (Figure 5a). This result is confirmed by early 2-deoxyglucose studies that suggest glucose uptake in glial cells of the ONL (Benson et al., 1985). Moreover, a morphological study shows the expression of glucose transporter-1 (GLUT-1) in OECs of the lamina propria (Nunez-Parra et al., 2011), supporting the notion that OECs possess the molecular machinery for glucose uptake at the BBB.

Our study shows that OECs in the outer ONL are part of a functional BBB, a hallmark exclusively attributed to astrocytes so far. Functional properties of perivascular OECs comprise glucose uptake and neurovascular coupling, capillaries in the ONL are surrounded by pericytes, and tight junctions between endothelial cells efficiently shield the neural parenchyma from noxious substances. Hence, the OEC-based BBB in the ONL shares the most important properties of the BBB in the rest of the brain.

CONFLICT OF INTEREST

The authors declare no conflict of interest.

DATA AVAILABILITY STATEMENT

The data that support the findings of this study are available from the corresponding author upon reasonable request.

ORCID

Antonia Beiersdorfer https://orcid.org/0000-0003-0976-005X
Frank Kirchhoff https://orcid.org/0000-0002-2324-2761
Christian Lohr https://orcid.org/0000-0001-6518-6422

REFERENCES

Abbott, N. J., Patabendige, A. A., Dolman, D. E., Yusof, S. R., & Begley, D. J. (2010). Structure and function of the blood-brain barrier. *Neurobiology of Disease*, *37*(1), 13–25. https://doi.org/10.1016/j.nbd.2009.07.030

Alarcon-Martinez, L., Yilmaz-Ozcan, S., Yemisci, M., Schallek, J., Kilic, K., Can, A., ... Dalkara, T. (2018). Capillary pericytes express alpha-smooth muscle actin, which requires prevention of filamentous-actin depolymerization for detection. *eLife*, *7*, 34861. https://doi.org/10.7554/eLife.34861

Armulik, A., Mae, M., & Betsholtz, C. (2011). Pericytes and the blood-brain barrier: Recent advances and implications for the delivery of CNS therapy. *Therapeutic Delivery*, *2*(4), 419–422.

Attwell, D., Buchan, A. M., Charpak, S., Lauritzen, M., Macvicar, B. A., & Newman, E. A. (2010). Glial and neuronal control of brain blood flow. *Nature*, *468*(7321), 232–243. https://doi.org/10.1038/nature09613

Attwell, D., Mishra, A., Hall, C. N., O'Farrell, F. M., & Dalkara, T. (2016). What is a pericyte? *Journal of Cerebral Blood Flow and Metabolism*, *36*(2), 451–455. https://doi.org/10.1177/0271678X15610340

Au, W. W., Treloar, H. B., & Greer, C. A. (2002). Sublaminar organization of the mouse olfactory bulb nerve layer. *The Journal of Comparative Neurology*, *446*(1), 68–80.

Bailey, M. S., & Shipley, M. T. (1993). Astrocyte subtypes in the rat olfactory bulb: Morphological heterogeneity and differential laminar distribution. *The Journal of Comparative Neurology, 328*(4), 501–526. https://doi.org/10.1002/cne.903280405

Ballabh, P., Braun, A., & Nedergaard, M. (2004). The blood-brain barrier: An overview: Structure, regulation, and clinical implications. *Neurobiology of Disease, 16*(1), 1–13. https://doi.org/10.1016/j.nbd.2003.12.016

Barnett, S. C., & Riddell, J. S. (2004). Olfactory ensheathing cells (OECs) and the treatment of CNS injury: Advantages and possible caveats. *Journal of Anatomy, 204*(1), 57–67. https://doi.org/10.1111/j.1469-7580.2004.00257.x

Barraud, P., Seferiadis, A. A., Tyson, L. D., Zwart, M. F., Szabo-Rogers, H. L., Ruhrberg, C., ... Baker, C. V. (2010). Neural crest origin of olfactory ensheathing glia. *Proceedings of the National Academy of Sciences of the United States of America, 107*(49), 21040–21045. https://doi.org/10.1073/pnas.1012248107

Barros, L. F., Courjaret, R., Jakoby, P., Loaiza, A., Lohr, C., & Deitmer, J. W. (2009). Preferential transport and metabolism of glucose in Bergmann glia over Purkinje cells: A multiphoton study of cerebellar slices. *Glia, 57*(9), 962–970. https://doi.org/10.1002/glia.20820

Barros, L. F., & Deitmer, J. W. (2010). Glucose and lactate supply to the synapse. *Brain Research Reviews, 63*(1–2), 149–159. https://doi.org/10.1016/j.brainresrev.2009.10.002

Beiersdorfer, A., Scheller, A., Kirchhoff, F., & Lohr, C. (2019). Panglial gap junctions between astrocytes and olfactory ensheathing cells mediate transmission of Ca(2+) transients and neurovascular coupling. *Glia, 67*(7), 1385–1400. https://doi.org/10.1002/glia.23613

Bell, R. D., Winkler, E. A., Sagare, A. P., Singh, I., LaRue, B., Deane, R., & Zlokovic, B. V. (2010). Pericytes control key neurovascular functions and neuronal phenotype in the adult brain and during brain aging. *Neuron, 68*(3), 409–427. https://doi.org/10.1016/j.neuron.2010.09.043

Benson, T. E., Burd, G. D., Greer, C. A., Landis, D. M., & Shepherd, G. M. (1985). High-resolution 2-deoxyglucose autoradiography in quick-frozen slabs of neonatal rat olfactory bulb. *Brain Research, 339*(1), 67–78.

Boyd, J. G., Skihar, V., Kawaja, M., & Doucette, R. (2003). Olfactory ensheathing cells: Historical perspective and therapeutic potential. *Anatomical Record. Part B, New Anatomist, 271*(1), 49–60. https://doi.org/10.1002/ar.b.10011

Brown, L. S., Foster, C. G., Courtney, J. M., King, N. E., Howells, D. W., & Sutherland, B. A. (2019). Pericytes and neurovascular function in the healthy and diseased brain. *Frontiers in Cellular Neuroscience, 13*, 282. https://doi.org/10.3389/fncel.2019.00282

Chaigneau, E., Oheim, M., Audinat, E., & Charpak, S. (2003). Two-photon imaging of capillary blood flow in olfactory bulb glomeruli. *Proceedings of the National Academy of Sciences of the United States of America, 100*(22), 13081–13086. https://doi.org/10.1073/pnas.2133652100

Chuquet, J., Quilichini, P., Nimchinsky, E. A., & Buzsaki, G. (2010). Predominant enhancement of glucose uptake in astrocytes versus neurons during activation of the somatosensory cortex. *The Journal of Neuroscience, 30*(45), 15298–15303. https://doi.org/10.1523/JNEUROSCI.0762-10.2010

Daneman, R., Zhou, L., Kebede, A. A., & Barres, B. A. (2010). Pericytes are required for blood-brain barrier integrity during embryogenesis. *Nature, 468*(7323), 562–566. https://doi.org/10.1038/nature09513

Dickinson, P. J., Griffiths, I. R., Barrie, J. M., Kyriakides, E., Pollock, G. F., & Barnett, S. C. (1997). Expression of the dm-20 isoform of the plp gene in olfactory nerve ensheathing cells: Evidence from developmental studies. *Journal of Neurocytology, 26*(3), 181–189. https://doi.org/10.1023/a:1018584013739

Doengi, M., Deitmer, J. W., & Lohr, C. (2008). New evidence for purinergic signaling in the olfactory bulb: A2A and P2Y1 receptors mediate intracellular calcium release in astrocytes. *The FASEB Journal, 22*(7), 2368–2378. https://doi.org/10.1096/fj.07-101782

Doengi, M., Hirnet, D., Coulon, P., Pape, H. C., Deitmer, J. W., & Lohr, C. (2009). GABA uptake-dependent Ca(2+) signaling in developing olfactory bulb astrocytes. *Proceedings of the National Academy of Sciences of the United States of America, 106*(41), 17570–17575. https://doi.org/10.1073/pnas.0809513106

Doucette, J. R. (1984). The glial cells in the nerve fiber layer of the rat olfactory bulb. *The Anatomical Record, 210*(2), 385–391. https://doi.org/10.1002/ar.1092100214

Doucette, R. (1990). Glial influences on axonal growth in the primary olfactory system. *Glia, 3*(6), 433–449. https://doi.org/10.1002/glia.440030602

Doucette, R. (1991). PNS-CNS transitional zone of the first cranial nerve. *The Journal of Comparative Neurology, 312*(3), 451–466. https://doi.org/10.1002/cne.903120311

Escartin, C., & Rouach, N. (2013). Astroglial networking contributes to neurometabolic coupling. *Frontiers in Neuroenergetics, 5*, 4. https://doi.org/10.3389/fnene.2013.00004

Filosa, J. A., Bonev, A. D., & Nelson, M. T. (2004). Calcium dynamics in cortical astrocytes and arterioles during neurovascular coupling. *Circulation Research, 95*(10), e73–e81. https://doi.org/10.1161/01.RES.0000148636.60732.2e

Gerhardt, H., & Betsholtz, C. (2003). Endothelial-pericyte interactions in angiogenesis. *Cell and Tissue Research, 314*(1), 15–23. https://doi.org/10.1007/s00441-003-0745-x

Giaume, C., Koulakoff, A., Roux, L., Holcman, D., & Rouach, N. (2010). Astroglial networks: A step further in neuroglial and gliovascular interactions. *Nature Reviews. Neuroscience, 11*(2), 87–99. https://doi.org/10.1038/nrn2757

Gordon, G. R., Mulligan, S. J., & MacVicar, B. A. (2007). Astrocyte control of the cerebrovasculature. *Glia, 55*(12), 1214–1221. https://doi.org/10.1002/glia.20543

Halasz, N., Ljungdahl, A., & Hokfelt, T. (1979). Transmitter histochemistry of the rat olfactory bulb III. Autoradiographic localization of [3H] GABA. *Brain Research, 167*(2), 221–240.

Hall, C. N., Reynell, C., Gesslein, B., Hamilton, N. B., Mishra, A., Sutherland, B. A., ... Attwell, D. (2014). Capillary pericytes regulate cerebral blood flow in health and disease. *Nature, 508*(7494), 55–60. https://doi.org/10.1038/nature13165

Hamilton, N. B., Attwell, D., & Hall, C. N. (2010). Pericyte-mediated regulation of capillary diameter: A component of neurovascular coupling in health and disease. *Frontiers in Neuroenergetics, 2*, 5. https://doi.org/10.3389/fnene.2010.00005

Harris, J. J., Jolivet, R., & Attwell, D. (2012). Synaptic energy use and supply. *Neuron, 75*(5), 762–777. https://doi.org/10.1016/j.neuron.2012.08.019

Hellstroem, M., Kalen, M., Lindahl, P., Abramsson, A., & Betsholtz, C. (1999). Role of PDGF-B and PDGFR-beta in recruitment of vascular smooth muscle cells and pericytes during embryonic blood vessel formation in the mouse. *Development, 126*(14), 3047–3055.

Herrera, L. P., Casas, C. E., Bates, M. L., & Guest, J. D. (2005). Ultrastructural study of the primary olfactory pathway in *Macaca fascicularis*. *The Journal of Comparative Neurology, 488*(4), 427–441. https://doi.org/10.1002/cne.20588

Hill, R. A., Tong, L., Yuan, P., Murikinati, S., Gupta, S., & Grutzendler, J. (2015). Regional blood flow in the Normal and ischemic brain is controlled by arteriolar smooth muscle cell contractility and not by capillary pericytes. *Neuron, 87*(1), 95–110. https://doi.org/10.1016/j.neuron.2015.06.001

Hirrlinger, P. G., Scheller, A., Braun, C., Quintela-Schneider, M., Fuss, B., Hirrlinger, J., & Kirchhoff, F. (2005). Expression of reef coral fluorescent proteins in the central nervous system of transgenic mice. *Molecular and Cellular Neurosciences, 30*(3), 291–303. https://doi.org/10.1016/j.mcn.2005.08.011

Hirschi, K. K., & D'Amore, P. A. (1996). Pericytes in the microvasculature. *Cardiovascular Research, 32*(4), 687–698.

Honore, A., Le Corre, S., Derambure, C., Normand, R., Duclos, C., Boyer, O., … Guerout, N. (2012). Isolation, characterization, and genetic profiling of subpopulations of olfactory ensheathing cells from the olfactory bulb. *Glia*, 60(3), 404–413. https://doi.org/10.1002/glia.22274

Jakoby, P., Schmidt, E., Ruminot, I., Gutierrez, R., Barros, L. F., & Deitmer, J. W. (2014). Higher transport and metabolism of glucose in astrocytes compared with neurons: A multiphoton study of hippocampal and cerebellar tissue slices. *Cerebral Cortex*, 24(1), 222–231. https://doi.org/10.1093/cercor/bhs309

Joost, E., Jordao, M. J. C., Mages, B., Prinz, M., Bechmann, I., & Krueger, M. (2019). Microglia contribute to the glia limitans around arteries, capillaries and veins under physiological conditions, in a model of neuroinflammation and in human brain tissue. *Brain Structure & Function*, 224(3), 1301–1314. https://doi.org/10.1007/s00429-019-01834-8

Kanda, T. (2013). Biology of the blood-nerve barrier and its alteration in immune mediated neuropathies. *Journal of Neurology, Neurosurgery, and Psychiatry*, 84(2), 208–212. https://doi.org/10.1136/jnnp-2012-302312

Lai, C. H., & Kuo, K. H. (2005). The critical component to establish in vitro BBB model: Pericyte. *Brain Research. Brain Research Reviews*, 50(2), 258–265. https://doi.org/10.1016/j.brainresrev.2005.07.004

Leone, D. P., Genoud, S., Atanasoski, S., Grausenburger, R., Berger, P., Metzger, D., … Suter, U. (2003). Tamoxifen-inducible glia-specific Cre mice for somatic mutagenesis in oligodendrocytes and Schwann cells. *Molecular and Cellular Neurosciences*, 22(4), 430–440.

Leybaert, L. (2005). Neurobarrier coupling in the brain: A partner of neurovascular and neurometabolic coupling? *Journal of Cerebral Blood Flow and Metabolism*, 25(1), 2–16. https://doi.org/10.1038/sj.jcbfm.9600001

Lindahl, P., Karlsson, L., Hellstrom, M., Gebre-Medhin, S., Willetts, K., Heath, J. K., & Betsholtz, C. (1997). Alveogenesis failure in PDGF-A-deficient mice is coupled to lack of distal spreading of alveolar smooth muscle cell progenitors during lung development. *Development*, 124(20), 3943–3953.

Lohr, C., Grosche, A., Reichenbach, A., & Hirnet, D. (2014). Purinergic neuron-glia interactions in sensory systems. *Pflügers Archiv: European Journal of Physiology*, 466(10), 1859–1872. https://doi.org/10.1007/s00424-014-1510-6

Longden, T. A., Dabertrand, F., Koide, M., Gonzales, A. L., Tykocki, N. R., Brayden, J. E., … Nelson, M. T. (2017). Capillary K(+)-sensing initiates retrograde hyperpolarization to increase local cerebral blood flow. *Nature Neuroscience*, 20(5), 717–726. https://doi.org/10.1038/nn.4533

Longden, T. A., Hill-Eubanks, D. C., & Nelson, M. T. (2016). Ion channel networks in the control of cerebral blood flow. *Journal of Cerebral Blood Flow and Metabolism*, 36(3), 492–512. https://doi.org/10.1177/0271678X15616138

Longden, T. A., & Nelson, M. T. (2015). Vascular inward rectifier K+ channels as external K+ sensors in the control of cerebral blood flow. *Microcirculation*, 22(3), 183–196. https://doi.org/10.1111/micc.12190

MacKenzie, M. L., Ghabriel, M. N., & Allt, G. (1987). The blood-nerve barrier: An in vivo lanthanum tracer study. *Journal of Anatomy*, 154, 27–37.

Madisen, L., Zwingman, T. A., Sunkin, S. M., Oh, S. W., Zariwala, H. A., Gu, H., … Zeng, H. (2010). A robust and high-throughput Cre reporting and characterization system for the whole mouse brain. *Nature Neuroscience*, 13(1), 133–140. https://doi.org/10.1038/nn.2467

Mulligan, S. J., & MacVicar, B. A. (2004). Calcium transients in astrocyte endfeet cause cerebrovascular constrictions. *Nature*, 431(7005), 195–199. https://doi.org/10.1038/nature02827

Nazareth, L., Chen, M., Shelper, T., Shah, M., Tello Velasquez, J., Walkden, H., … Ekberg, J. A. K. (2019). Novel insights into the glia limitans of the olfactory nervous system. *The Journal of Comparative Neurology*, 527(7), 1228–1244. https://doi.org/10.1002/cne.24618

Nico, B., Frigeri, A., Nicchia, G. P., Quondamatteo, F., Herken, R., Errede, M., … Roncali, L. (2001). Role of aquaporin-4 water channel in the development and integrity of the blood-brain barrier. *Journal of Cell Science*, 114(Pt 7), 1297–1307.

Nielsen, S., Nagelhus, E. A., Amiry-Moghaddam, M., Bourque, C., Agre, P., & Ottersen, O. P. (1997). Specialized membrane domains for water transport in glial cells: High-resolution immunogold cytochemistry of aquaporin-4 in rat brain. *The Journal of Neuroscience*, 17(1), 171–180.

Nunez-Parra, A., Cortes-Campos, C., Bacigalupo, J., Garcia Mde, L., Nualart, F., & Reyes, J. G. (2011). Expression and distribution of facilitative glucose (GLUTs) and monocarboxylate/H+ (MCTs) transporters in rat olfactory epithelia. *Chemical Senses*, 36(9), 771–780. https://doi.org/10.1093/chemse/bjr052

Pellerin, L., Bouzier-Sore, A. K., Aubert, A., Serres, S., Merle, M., Costalat, R., & Magistretti, P. J. (2007). Activity-dependent regulation of energy metabolism by astrocytes: An update. *Glia*, 55(12), 1251–1262. https://doi.org/10.1002/glia.20528

Petzold, G. C., Albeanu, D. F., Sato, T. F., & Murthy, V. N. (2008). Coupling of neural activity to blood flow in olfactory glomeruli is mediated by astrocytic pathways. *Neuron*, 58(6), 897–910. https://doi.org/10.1016/j.neuron.2008.04.029

Piantanida, A. P., Acosta, L. E., Brocardo, L., Capurro, C., Greer, C. A., & Rela, L. (2019). Selective Cre-mediated gene deletion identifies connexin 43 as the main connexin channel supporting olfactory ensheathing cell networks. *The Journal of Comparative Neurology*, 527(7), 1278–1289. https://doi.org/10.1002/cne.24628

Raponi, E., Agenes, F., Delphin, C., Assard, N., Baudier, J., Legraverend, C., & Deloulme, J. C. (2007). S100B expression defines a state in which GFAP-expressing cells lose their neural stem cell potential and acquire a more mature developmental stage. *Glia*, 55(2), 165–177. https://doi.org/10.1002/glia.20445

Rash, J. E., & Yasumura, T. (1999). Direct immunogold labeling of connexins and aquaporin-4 in freeze-fracture replicas of liver, brain, and spinal cord: Factors limiting quantitative analysis. *Cell and Tissue Research*, 296(2), 307–321.

Rela, L., Bordey, A., & Greer, C. A. (2010). Olfactory ensheathing cell membrane properties are shaped by connectivity. *Glia*, 58(6), 665–678. https://doi.org/10.1002/glia.20953

Rela, L., Piantanida, A. P., Bordey, A., & Greer, C. A. (2015). Voltage-dependent K+ currents contribute to heterogeneity of olfactory ensheathing cells. *Glia*, 63(9), 1646–1659. https://doi.org/10.1002/glia.22834

Rieger, A., Deitmer, J. W., & Lohr, C. (2007). Axon-glia communication evokes calcium signaling in olfactory ensheathing cells of the developing olfactory bulb. *Glia*, 55(4), 352–359. https://doi.org/10.1002/glia.20460

Rotermund, N., Schulz, K., Hirnet, D., & Lohr, C. (2019). Purinergic signaling in the vertebrate olfactory system. *Frontiers in Cellular Neuroscience*, 13, 112. https://doi.org/10.3389/fncel.2019.00112

Rungta, R. L., Chaigneau, E., Osmanski, B.-F., & Charpak, S. J. N. (2018). Vascular compartmentalization of functional hyperemia from the synapse to the pia, 99(2), 362–375. e364.

Sharp, F. R., Kauer, J. S., & Shepherd, G. M. (1977). Laminar analysis of 2-deoxyglucose uptake in olfactory bulb and olfactory cortex of rabbit and rat. *Journal of Neurophysiology*, 40(4), 800–813. https://doi.org/10.1152/jn.1977.40.4.800

Shepherd, G. M. (2003). The single capillary and the active brain. *Proceedings of the National Academy of Sciences of the United States of America*, 100(22), 12535–12536. https://doi.org/10.1073/pnas.2336089100

Simard, M., Arcuino, G., Takano, T., Liu, Q. S., & Nedergaard, M. (2003). Signaling at the gliovascular interface. *The Journal of Neuroscience*, 23(27), 9254–9262.

Simpson, I. A., Carruthers, A., & Vannucci, S. (2007). Supply and demand in cerebral energy metabolism: The role of nutrient transporters. *Journal of Cerebral Blood Flow and Metabolism*, 27(11), 1766–1791.

Smith, G. M., Falone, A. E., & Frank, E. (2012). Sensory axon regeneration: Rebuilding functional connections in the spinal cord. *Trends in Neurosciences*, 35(3), 156–163. https://doi.org/10.1016/j.tins.2011.10.006

Smits, A., Kato, M., Westermark, B., Nister, M., Heldin, C. H., & Funa, K. (1991). Neurotrophic activity of platelet-derived growth factor (PDGF): Rat neuronal cells possess functional PDGF beta-type receptors and respond to PDGF. *Proceedings of the National Academy of Sciences of the United States of America*, 88(18), 8159–8163. https://doi.org/10.1073/pnas.88.18.8159

Stavermann, M., Buddrus, K., St John, J. A., Ekberg, J. A., Nilius, B., Deitmer, J. W., & Lohr, C. (2012). Temperature-dependent calcium-induced calcium release via InsP3 receptors in mouse olfactory ensheathing glial cells. *Cell Calcium*, 52(2), 113–123. https://doi.org/10.1016/j.ceca.2012.04.017

Stavermann, M., Meuth, P., Doengi, M., Thyssen, A., Deitmer, J. W., & Lohr, C. (2015). Calcium-induced calcium release and gap junctions mediate large-scale calcium waves in olfactory ensheathing cells in situ. *Cell Calcium*, 58(2), 215–225. https://doi.org/10.1016/j.ceca.2015.05.003

Stosiek, C., Garaschuk, O., Holthoff, K., & Konnerth, A. (2003). In vivo two-photon calcium imaging of neuronal networks. *Proceedings of the National Academy of Sciences of the United States of America*, 100(12), 7319–7324. https://doi.org/10.1073/pnas.1232232100

Takano, T., Tian, G. F., Peng, W., Lou, N., Libionka, W., Han, X., & Nedergaard, M. (2006). Astrocyte-mediated control of cerebral blood flow. *Nature Neuroscience*, 9(2), 260–267. https://doi.org/10.1038/nn1623

Thyssen, A., Hirnet, D., Wolburg, H., Schmalzing, G., Deitmer, J. W., & Lohr, C. (2010). Ectopic vesicular neurotransmitter release along sensory axons mediates neurovascular coupling via glial calcium signaling. *Proceedings of the National Academy of Sciences of the United States of America*, 107(34), 15258–15263. https://doi.org/10.1073/pnas.1003501107

Thyssen, A., Stavermann, M., Buddrus, K., Doengi, M., Ekberg, J. A., St John, J. A., ... Lohr, C. (2013). Spatial and developmental heterogeneity of calcium signaling in olfactory ensheathing cells. *Glia*, 61(3), 327–337. https://doi.org/10.1002/glia.22434

Vanlandewijck, M., & Betsholtz, C. (2018). Single-cell mRNA sequencing of the mouse brain vasculature. *Methods in Molecular Biology*, 1846, 309–324. https://doi.org/10.1007/978-1-4939-8712-2_21

Windus, L. C., Lineburg, K. E., Scott, S. E., Claxton, C., Mackay-Sim, A., Key, B., & St John, J. A. (2010). Lamellipodia mediate the heterogeneity of central olfactory ensheathing cell interactions. *Cellular and Molecular Life Sciences*, 67(10), 1735–1750. https://doi.org/10.1007/s00018-010-0280-3

Winkler, E. A., Bell, R. D., & Zlokovic, B. V. (2010). Pericyte-specific expression of PDGF beta receptor in mouse models with normal and deficient PDGF beta receptor signaling. *Molecular Neurodegeneration*, 5, 32. https://doi.org/10.1186/1750-1326-5-32

Winkler, E. A., Birk, H., Burkhardt, J. K., Chen, X., Yue, J. K., Guo, D., ... Lawton, M. T. (2018). Reductions in brain pericytes are associated with arteriovenous malformation vascular instability. *Journal of Neurosurgery*, 129(6), 1464–1474. https://doi.org/10.3171/2017.6.JNS17860

Wolburg, H., & Lippoldt, A. (2002). Tight junctions of the blood-brain barrier: Development, composition and regulation. *Vascular Pharmacology*, 38(6), 323–337.

Wolburg, H., Wolburg-Buchholz, K., Fallier-Becker, P., Noell, S., & Mack, A. F. (2011). Structure and functions of aquaporin-4-based orthogonal arrays of particles. *International Review of Cell and Molecular Biology*, 287, 1–41. https://doi.org/10.1016/B978-0-12-386043-9.00001-3

Wolburg, H., Wolburg-Buchholz, K., Sam, H., Horvat, S., Deli, M. A., & Mack, A. F. (2008). Epithelial and endothelial barriers in the olfactory region of the nasal cavity of the rat. *Histochemistry and Cell Biology*, 130(1), 127–140. https://doi.org/10.1007/s00418-008-0410-2

Zhao, Z., Nelson, A. R., Betsholtz, C., & Zlokovic, B. V. (2015). Establishment and dysfunction of the blood-brain barrier. *Cell*, 163(5), 1064–1078. https://doi.org/10.1016/j.cell.2015.10.067

Zonta, M., Angulo, M. C., Gobbo, S., Rosengarten, B., Hossmann, K. A., Pozzan, T., & Carmignoto, G. (2003). Neuron-to-astrocyte signaling is central to the dynamic control of brain microcirculation. *Nature Neuroscience*, 6(1), 43–50. https://doi.org/10.1038/nn980

SUPPORTING INFORMATION

Additional supporting information may be found online in the Supporting Information section at the end of this article.